Urban Air Quality Modeling Using Low-Cost Sensor Network and Data Assimilation in the Aburrá Valley, Colombia

Santiago Lopez-Restrepo[a,c,e,*], Andres Yarce[a,c,e], Nicolás Pinel[b], O. L. Quintero[a], Arjo Segers[d] and A. W. Heemink[c]

[a]*Mathematical Modelling Research Group at Universidad EAFIT. Medellín Colombia.*
[b]*Department of Biological Sciences; Research Group on Biodiversity, Evolution and Conservation at Universidad EAFIT. Medellín, Colombia.*
[c]*Department of Applied Mathematics at TU Delft. Delft, The Netherlands.*
[d]*TNO Department of Climate, Air and Sustainability. Utrecht, The Netherlands.*
[e]*SimpleSpace. Medellín, Colombia.*

ARTICLE INFO

Keywords:
low-cost network, Chemistry Transport Model, Data assimilation, Particulate Matter,Citizen Scientists

ABSTRACT

The use of low air quality networks has been increasing in recent years to study urban pollution dynamics. Here we show the evaluation of the operational Aburrá Valley's low-cost network against the official monitoring network. The results show that the $PM_{2.5}$ low-cost measurements are very close to those observed by the official network. Additionally, the low-cost allows a higher spatial representation of the concentrations across the valley. We integrate low-cost observations with the chemical transport model LOTOS-EUROS using data assimilation. Two different configurations of the low-cost network were assimilated: using the whole low-cost network (255 sensors), and a high-quality using just the sensors with a correlation factor greater than 0.8 with respect to the official network (115 sensors). The official stations were also assimilated to compare the more dense low-cost network's impact on the model performance. Both simulations assimilating the low-cost model outperform the model without assimilation and assimilating the official network. The model capability to predict high concentration events' warnings is also improved by assimilating the low-cost network with respect to the other simulations. Finally, the simulation using the high-quality configuration has lower error values than using the complete low-cost network, showing that it is essential to consider the quality and location and not just the total number of sensors. Our results suggest that with the current advance in low-cost sensors, it is possible to improve model performance with low-cost network data assimilation.

1. Introduction

Particulate matter (PM) is one of the most problematic pollutants in urban air (Liu, Bartonova, Schindler, Sharma, Behera, Katiyar and Dikshit, 2013). The effects of PM on human health, associated especially with PM of $\leq 2.5\mu$m in diameter, include asthma, lung cancer and cardiovascular disease (Liu, Dunea, Iordache and Pohoata, 2018). Consequently, major urban centers commonly monitor $PM_{2.5}$ as part of their air quality management strategies.

Public air quality monitoring networks often consist of fixed measuring stations equipped with expensive sensors and maintained under rigorous operational and calibration regimes in order to provide high quality data. The high costs associated with establishing and maintaining such stations means that not all cities in developing countries can afford monitoring networks of sufficient spatial coverage (Kumar and Gurjar, 2019). Even in large cities in developed countries, the official air quality monitoring networks do not always provide information at the spatial and temporal resolution required to assess the impact of pollution sources on health (Ahangar, Freedman and Venkatram, 2019), as the cost of the equipment makes the necessary density prohibitive. This has motivated the expansion and improvement of low-cost systems and programs to measure PM. The limited number of studies that have evaluated newer generations of low-cost $PM_{2.5}$ sensors have shown that the most widely used low-cost sensors attain high accuracy when compared to standard monitoring stations (R^2 value ranging from 0.93 to 0.95) (Liu, Schneider, Haugen and Vogt, 2019). The data provided by these sensors can complement those generated by conventional systems, increasing the data resolution and allowing studies of exposure at the human level (Schneider, Castell, Vogt, Dauge, Lahoz and Bartonova, 2017; Ahangar et al., 2019).

* Corresponding author. slopezr2@eafit.edu.co,s.lopezrestrepo@tudelft.nl (S. Lopez-Restrepo)
ORCID(s): 0000-0002-7637-1575 (S. Lopez-Restrepo); 0000-0003-1441-2367 (A. Yarce); 0000-0003-1304-3096 (N. Pinel); 0000-0002-8697-4361 (O.L. Quintero); 0000-0002-1319-0195 (A. Segers); 0000-0001-8559-9566 (A.W. Heemink)

The integration of observations from dense networks of low-cost sensors into mathematical models through techniques such as data fusion or data assimilation enables a spatially continuous representation of concentration fields with significantly reduced bias (Lahoz and Schneider, 2014). These techniques provide an added value to the sensor observations by spatially interpolating between monitoring locations and at the same time adding value to the model by constraining the model with observations. Both sources of information can thus be combined in a mathematically objective manner with the goal of reducing the uncertainty inherent to both sources (Schneider et al., 2017; Liu et al., 2019; Popoola, Carruthers, Lad, Bright, Mead, Stettler, Saffell and Jones, 2018). Although data assimilation is a more complex family of methods than data fusion or interpolation techniques, it is by far the most versatile and the robust of these approaches (Lahoz and Schneider, 2014).

This work seeks to implement the data assimilation technique *Ensemble Kalman Filter* (EnKF) (Evensen, 2003) to integrate data from a hyper-dense, low-cost $PM_{2.5}$ measuring network operated in Medellín (Colombia) and its neighboring municipalities of the Aburrá Valley (Hoyos, Herrera-Mejía, Roldán-Henao and Isaza, 2019) into the Chemical Transport Model LOTOS-EUROS (Manders, Builtjes, Curier, Denier Van Der Gon, Hendriks, Jonkers, Kranenburg, Kuenen, Segers, Timmermans, Visschedijk, Kruit, Addo, Van Pul, Sauter, Van Der Swaluw, Swart, Douros, Eskes, Van Meijgaard, Van Ulft, Van Velthoven, Banzhaf, Mues, Stern, Fu, Lu, Heemink, Van Velzen and Schaap, 2017). Data generated by the robust, official network of air quality monitoring stations in the Aburrá Valley were previously used for data assimilation in LOTOS-EUROS for modelling and forecasting PM dynamics in the valley (Lopez-Restrepo, Yarce, Pinel, Quintero, Segers and Heemink, 2020). The goal with using data from the low-cost sensor network is to evaluate the impact of hyper-dense observations in the data assimilation approach and their viability as an alternative to monitoring $PM_{2.5}$ concentrations in developing countries. This study differs from previous studies such as (Schneider et al., 2017; Ahangar et al., 2019; Popoola et al., 2018; Pournazeri, Tan, Schulte, Jing and Venkatram, 2014), in which a dispersion model was used to construct concentration maps or to estimate emissions from the measured concentration fields, and the integration of the model and observations was based on Kriging or other static approaches. In this work a dynamic data assimilation method is implemented to guide the model's concentration fields using the observations.

The main contributions from this work are as follows: 1) an evaluation of the low-cost sensor network against the official network; 2) the implementation of techniques for the assimilation of low-cost high-density data, focusing on the impact on the assimilated model results; and 3) a methodology for performing and evaluating PM forecasts with assimilated data over three-day windows, providing valuable information for decision makers. The paper is organized as follow: Section 2 describes the low-cost network, the LOTOS-EUROS model and the basic concepts of the the Ensemble Kalman Filter; Section 3 presents the results of the low-cost network evaluation, the data assimilation and forecast experiments; Section 4 discusses the results and important remarks; and lastly, Section 5 presents the conclusions and needed future work.

2. Materials and methods

The period of interest for all data evaluations, simulations and data assimilation experiments spans from February 25 to March 15, 2019. During these days, the air quality in the Aburrá Valley worsened due to the Northbound transit of the Inter-Tropical Convergence Zone.

2.1. Hyper-dense low-cost sensor network

In Medellín and its greater metropolitan area inside the Aburrá Valley, the *Sistema de Alerta Temprana del Valle de Aburrá* (SIATA, `www.siata.gov.co`) project operates the official high-end air quality monitoring network (henceforth *official network*, and a hyper-dense, low-cost air quality network developed within the Citizen Scientist program (henceforth *low-cost network*).

The official network provides high quality measurements for different pollutants in the atmosphere over the Aburrá Valley such as O_3, SO_2, PM_{10}, $PM_{2.5}$ and PM_1. The official network is distributed among the ten municipalities of the Valley, with the majority of the stations located within the city of Medellín (Figure 1, panel a). The PM measurement equipment consists of Met One Instruments BAM-1020 and BAM-1022 that produce averaged hourly data Hoyos et al. (2019).

The low-cost network was created with the aim of engaging the community in issues surrounding air quality, and as an extension of the official network. As of writing, the low-cost network consists of 255 real-time $PM_{2.5}$ sensors across the Aburrá Valley and its hills. They are located in the premises of private homes and public or private institutions (Figure 1, panel b). Measurements are generated with a 1-minute temporal resolution. The measuring equipment was

(a) Official monitoring network (b) Low-cost network

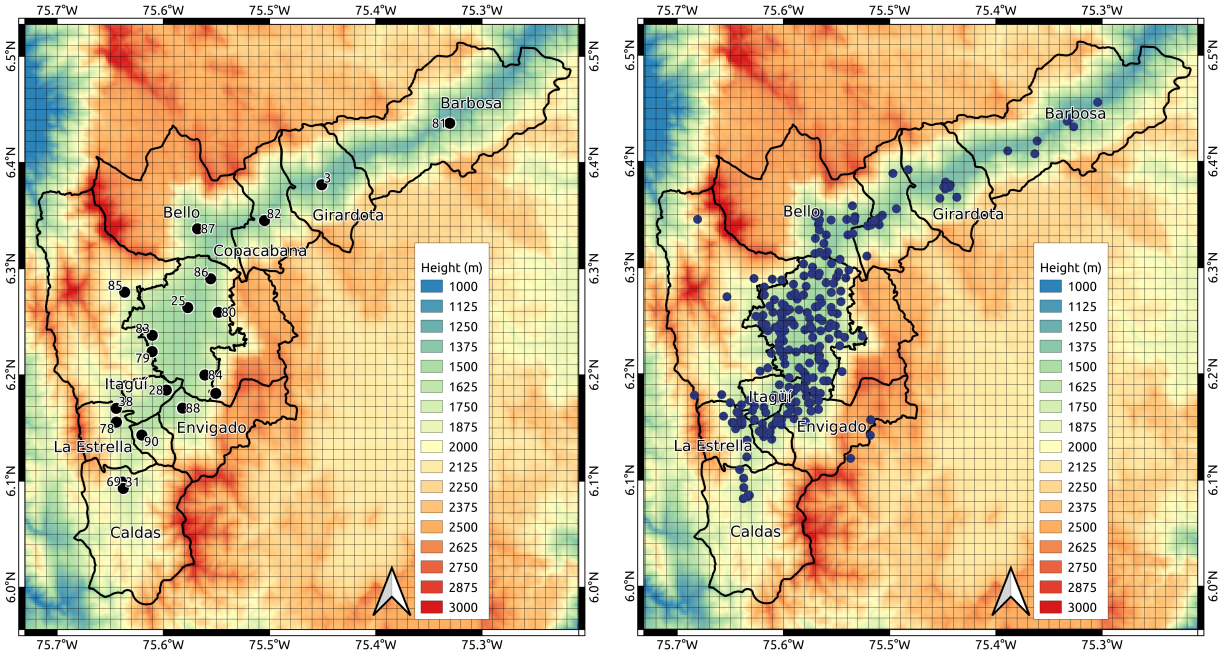

Figure 1: Spatial distribution of the hyper-dense low-cost network Citizen Scientist and official monitoring air-quality network for $PM_{2.5}$. The gray raster represent the LOTOS-EUROS model grid.

developed by SIATA based on the well-known low-cost Shinyei PPD42NS, NOVA SDS011, and Bjhike HK-A5 sensors (Hoyos et al., 2019). The NOVA SDS011 measurements have shown a good correlation with reference monitoring stations, and their data show high potential for research purposes (Liu et al., 2019). Each low-cost sensor is calibrated individually against BAM-1020 measurements (Hoyos et al., 2019). The calibration process showed the measurements of 91% of the low-cost sensors with correlation values above 0.6 against the official measurements, and 67% with values above 0.8. The median of the root mean square error showed a value of 6.2 $\mu g/m^3$, with a tendency to decrease for higher concentrations Hoyos et al. (2019). The low-cost network thus represents satisfactorily the dynamics of $PM_{2.5}$ concentrations in the Valley's atmosphere.

Data were downloaded from SIATA's data portal, available at `https://siata.gov.co/descarga_siata/index.php/index2/`. Data from the official network for the corresponding dates were used for validation of both the low-cost network and the model simulations before and after data assimilation. Each station from the official network served as a reference point for all low-cost network sensors within a 2-km radius of the former. Performance of the latter was evaluated using as metrics the Mean Fractional Bias (MFB), the Root Mean Square Error (RMSE) and the Pearson correlation coefficient (R) (Chai and Draxler, 2014; Boylan and Russell, 2006; Shaocai, Brian, Robin, Shao-Hang and E., 2006). When a low-cost sensors had more than one official station within a 2-km radius, the average value of the official measurements was used.

2.2. Particulate Matter Modelling

2.2.1. LOTOS-EUROS Model

The LOTOS-EUROS (LOng Term Ozone Simulation-EURopean Operational Smog model) (Mues, Kuenen, Hendriks, Manders, Segers, Scholz, Hueglin, Builtjes and Schaap, 2014) is a chemical transport model that simulates concentrations of gasses and aerosols in the lower troposphere on a 3D grid. The simulated species include ozone, nitrogen oxides, volatile organic compounds, secondary inorganic aerosols, dust, and sea-salt (Sauter, der Swaluw, Manders-groot, Kruit, Segers and Eskes, 2012). The dynamics are regulated by processes such as chemical reactions, diffusion, drag, dry and wet deposition, emissions and advection (Van Loon, Builtjes and Segers, 2000).

Simulations were conducted using a one-way nested domain configuration as shown in Figure 2 and detailed in Table 1. The innermost domain (D4), the focus of the present study, covers the Aburrá Valley with a model resolution

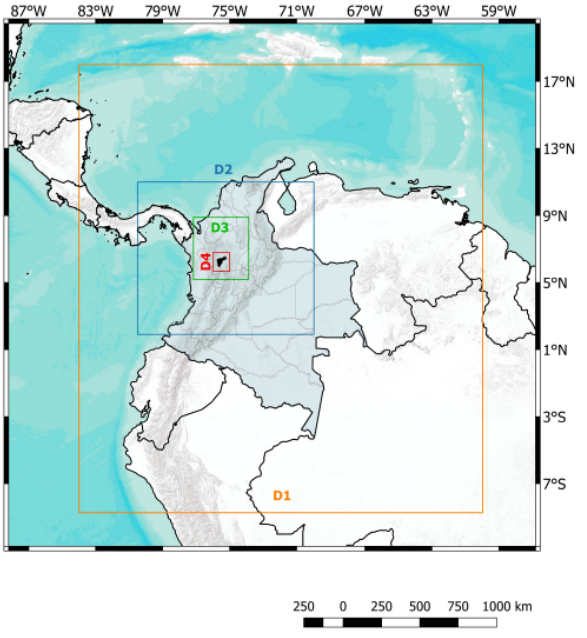

Figure 2: Nested domain configuration for LOTOS-EUROS simulations. All the experiment presented in this work are performed in the domain D4.

of 0.01° (about 1 km × 1 km) as shown in Figure 1. The anthropogenic emissions input for D4 were updated with a high-resolution local emissions inventory constructed as described in Section 2.2.2. The model set up is summarized in Table 2 (for details, see (Lopez-Restrepo et al., 2020)).

Domain	Longitude	Latitude	Cell size
D1	84°W-60°W	8.5°S-18°N	0.27°× 0.27°
D2	80.5°W-70°W	2°N-11°N	0.09°× 0.09°
D3	77.2°W-73.9°W	5.2°N-8.9°N	0.03°× 0.03°
D4	76°W-75°W	5.7°N-6.8°N	0.01°× 0.01°

Table 1
One-way nested domain configuration used for simulations in LOTOS-EUROS. All data assimilation experiments were conducted in D4.

	D1	D2	D3	D4
Boundary conditions	CAMS 1.4° × 1.4°	D1 0.27°×0.27°	D2 0.09 °× 0.09°	D3 0.03°×0.03°
Meteorology	ECMWF 1.4° × 1.4°		ECMWF 0.07° × 0.07°	
Anthropogenic emissions	EDGAR V4.2 $0.1^o \times 0.1^o$			Local EI $0.01^o \times 0.01^o$
Biogenic emissions	MEGAN $0.1^o \times 0.1^o$			
Fire emissions	CAMS GFAS $0.1^o \times 0.1^o$			
Land use	GLC2000 $0.01^o \times 0.01^o$			
Orography	GMTED2010 0.002° × 0.002°			

Table 2
LOTOS-EUROS simulations set-up. LOTOS-EUROS outputs are written each hour. Meteorological data presents a temporal resolution of 3 hours.

2.2.2. Local Emissions Inventory

An anthropogenic urban emissions inventory for 2016 specific to Medellín and the other nine municipalities of the Aburrá Valley was used for the simulations on the D4 domain. This inventory provides a complete set of emitted trace gases such as carbon monoxide (CO), nitrogen oxides (NO_x), sulphur oxides (SO_x), and volatile organic compounds (VOC's), as well as particulate matter with diameter less than 2.5 μm ($PM_{2.5}$) or less than 10 μm (PM_{10}). The construction of the inventory followed a bottom-up methodology, combining activity data (traffic intensities, industrial production) with emission factors. Only traffic and industrial point sources were considered, without accounting for neither household nor commercial emissions (UPB and AMVA, 2017).

For integration into LOTOS-EUROS, the emissions inventory was disaggregated over the Aburrá Valley (76°W-75°W and 5.7°N-6.8°N) at a resolution of 0.01°× 0.01°(approximately 1 km × 1 km), using a method based on road density as in Ossés de Eicker, Zah, Triviño and Hurni (2008). The road network map was obtained from the OpenStreetMap database (Haklay and Weber, 2008), and simplified by removing segments classified as residential, as recommended in (Tuia, Ossés de Eicker, Zah, Osses, Zarate and Clappier, 2007; Gómez, González, Osses and Aristizábal, 2018). The simplification of the road network can reduce errors in the spatial disaggregation since residential roads correspond to a high portion of the road network length but carry a low percentage of total vehicular traffic. For each grid cell j, the corresponding dissagregation factor DF was calculated as in (Ossés de Eicker et al., 2008). Namely,

$$DF_j = \frac{\sum_{i=0}^{I} S_{i,j}}{\sum_{j=0}^{J}\sum_{i=0}^{I} S_{i,j}} \tag{1}$$

where $S_{i,j}$ is the length of road segment i in the grid cell j, I is the number of road segments in cell j, and J is the total number of grid cells. The point-source emissions were distributed on the grid using their known location, obtained from the official emissions inventory (UPB and AMVA, 2017). Figure 3 shows the resulting emissions maps for $PM_{2.5}$ and PM_{10}.

(a) $PM_{2.5}$.

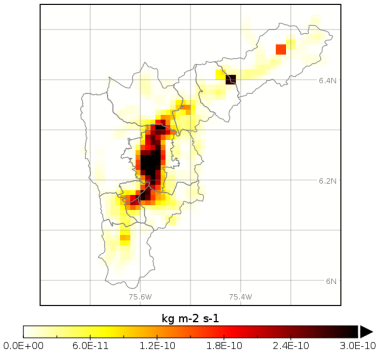

(b) PM_{10}.

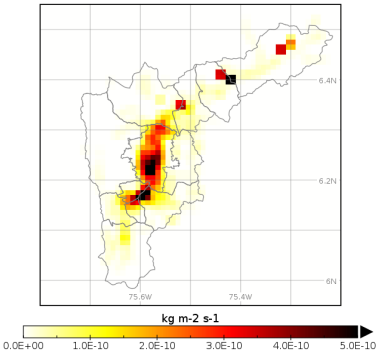

Figure 3: Local particulate matter emission inventories for the Aburrá Valley: (a) $PM_{2.5}$, and (b) PM_{10}. The values correspond with the estimated annual emissions.

2.3. Ensemble Kalman Filter

The Ensemble Kalman Filter (EnKF) is a Monte Carlo ensemble method, based on the approximation of the state probability density through an ensemble of model realizations (Evensen, 2003). The EnKF is initialized by generating a random ensemble of the model states that represents the model's uncertainty:

$$\xi_1^a, \ldots, \xi_N^a \tag{2}$$

Since emissions are a major source of uncertainty in air quality modelling, we generate the ensembles from perturbations in the emissions. Each ensemble member is propagated in time by the model M to obtain a forecast ensemble:

$$\boldsymbol{\xi}_k^{f(i)} \;=\; \boldsymbol{M}(\boldsymbol{\xi}_{k-1}^{a(i)}), \tag{3}$$

where $\boldsymbol{\xi}_k^{f(i)}$ is the $i-th$ member of the forecast ensemble at time k. The forecast ensemble describes a stochastic distribution with mean and covariance available from:

$$\boldsymbol{x}_k^f \;=\; \frac{1}{N}\sum_{i=1}^{N}\boldsymbol{\xi}_k^{f(i)}, \tag{4}$$

$$\boldsymbol{P}_k^f \;=\; \left[\boldsymbol{L}_k^f\left(\boldsymbol{L}_k^f\right)^T\right]/(N-1), \tag{5}$$

with N being the number of ensemble members. The matrix $\boldsymbol{L}$ is formed by deviations of the ensemble members from the mean:

$$\boldsymbol{L}_{\boldsymbol{k}}^{\boldsymbol{f}} = \left[\boldsymbol{\xi}_k^{f(1)} - \boldsymbol{x}_k^f, \ldots, \boldsymbol{\xi}_k^{f(N)} - \boldsymbol{x}_k^f\right]. \tag{6}$$

Most of the data assimilation applications do not calculate the matrix $\boldsymbol{P}^f$ directly due to its large size. Instead, a consistent square root formulation that only uses and stores $\boldsymbol{L}^f$ is computed (Tippett, Anderson, Bishop, Hamill and Whitaker, 2003) in the operational code. The EnKF uses observations $\boldsymbol{y}_k$ to update the forecast ensemble into a corrected or analysis ensemble. Observations collected in a vector $\boldsymbol{y}_k$ are represented as a linear mapping from the state vector plus an observation representation error:

$$\boldsymbol{y}_k \;=\; \boldsymbol{H}_k\,\boldsymbol{x}_k + \boldsymbol{v}_k, \quad \boldsymbol{v}_k \sim N(0, \boldsymbol{R}_k). \tag{7}$$

The observation operator H maps the state into the observations. In this application, H selects the concentration in locations where the observations are available. The representation error $\boldsymbol{v}_k$ describes the difference between observation and simulation due to both instrument and sampling errors. $\boldsymbol{v}_k$ is defined as a Gaussian noise with mean 0 and standard deviation depending on the measurement instrument. The analysis ensemble members are calculated following:

$$\boldsymbol{\xi}_k^{a(i)} \;=\; \boldsymbol{\xi}_k^{f(i)} + \boldsymbol{K}_k\left[\,\boldsymbol{y}_k \;-\; \boldsymbol{H}_k\boldsymbol{\xi}_k^{f(i)} \;+\; \boldsymbol{v}_k^{(i)}\right], \tag{8}$$

with

$$\boldsymbol{K}_k \;=\; \boldsymbol{P}_k^f\boldsymbol{H}_k^T[\boldsymbol{H}_k\boldsymbol{P}_k^f\boldsymbol{H}_k^T + \boldsymbol{R}_k]^{-1}. \tag{9}$$

The EnKF system in this application is configured to obtain estimates of both concentrations and emissions. An augmented state vector is used combining the $PM_{2.5}$ concentrations (c), propagated in time by LOTOS-EUROS, and emission correction factors (δe), propagated in time by a colored noise model (Jazwinski, 1970):

$$\begin{bmatrix}\boldsymbol{c}_k\\ \boldsymbol{\delta e}_k\end{bmatrix} = \begin{bmatrix}\boldsymbol{M}_{LE}\left(\boldsymbol{c}_{k-1}, \boldsymbol{\delta e}_{k-1}\right)\\ \boldsymbol{\delta e}_{k-1}\cdot\exp\left(-1/\tau\right)\end{bmatrix} + \begin{bmatrix}0\\ \sigma\cdot\sqrt{1-\alpha^2}\end{bmatrix}\boldsymbol{w}_k, \tag{10}$$

where M_{LE} is the LOTOS-EUROS model, τ and σ are the correlation length and variance of the stochastic process, and $\boldsymbol{w}_k$ is standard white noise sample. The emissions ($\hat{e}$) are calculated as:

$$\hat{\boldsymbol{e}} \;=\; \boldsymbol{e}\cdot\boldsymbol{\delta e}, \tag{11}$$

where $\boldsymbol{e}$ represents the nominal emissions from the emissions inventory. For all the simulations we used a τ of 1 day and a σ of 0.5 following previous results (Lopez-Restrepo et al., 2020). Additionally, we used a covariance localization scheme to reduce spurious correlations among distant states. The covariance localization technique artificially reduces the covariance between states that are separated by longer distances than a threshold radius ρ (Ott, Hunt, Szunyogh,

Zimin, Kostelich, Corazza, Kalnay, Patil and Yorke, 2004; Sakov, Evensen and Bertino, 2010). The parameter ρ defines the area of influence of a given observation on the concentrations and emissions to be estimated. We defined a localization radius ρ =5 km for all the simulations. We used an ensemble of N =25 members. Additional experiments with larger ensembles were performed without improvements in performance (not shown).

Two sets of low-cost sensors data were assembled: The first one included 255 sensors from the low-cost network that had a station from the official network within a 2-km radius. The second, higher quality one consisted of a subset of the previous set, including only those sensors whose data showed an R value equal or greater than 0.8 when evaluated against the official network.

We performed four different LOTOS-EUROS simulations:

1. a LOTOS-EUROS model simulation without data assimilation (henceforth *LE*);
2. a simulation with assimilation of data (observations) from the 14 stations of the official network (henceforth *LE-official*. The 14 stations were selected randomly and are indicated as red squares in Figure 6);
3. a simulation with assimilation of the data from the entire low-cost network (henceforth *LE-lowcost*)
4. a simulation with assimilation only of high-quality data from the low-cost network (henceforth *LE-lowcost-HQ*).

The 7 stations from the official network that were not used for data assimilation (green stars in Figure 6) were used as validation stations for all simulations.

2.4. Forecast experiments

Data assimilation can improve forecast performance mainly for two reasons: First, if the simulation is initialed with an assimilated field value, initial conditions at the start of the forecast window be a representation closer to reality than what the model alone may provide; second, the emission correction factors that were included in the assimilation state (10) can be applied to the model during the forecast window to adjust the emissions in the same direction as during assimilation.

Forecasting experiments were conducted to evaluate the capabilities of the model with data assimilation to forecast PM concentrations in the valley up to three days. Simulations were carried out as above, with the assimilation schedule illustrated in Figure 4. Data assimilation was conducted up to the indicated date, with the three subsequent days representing the forecast window. The forecasting window started at 00:00 hours of the first day after the end of data assimilation. To bring the information obtained in the assimilation window into the forecast window, we used the hourly profile of the correction factor calculated from the last 24 hours of data assimilation. The experiments continued until all days between March 9 and March 13 (inclusive) had predictions as the first, second and third day of the forecast. The performance of the forecast was evaluated by calculating the Air Quality Index (AQI) according to the ranges established by the Metropolitan Area [1] and illustrated in Table 3; and comparing it to the AQI observed for the corresponding day. The comparison against the AQI rather than against plain PM concentrations facilitates the interpretation of the model forecast performance by decision makers and the general public. Additionally, this representation affords evaluating the ability of the model to predict warning-triggering episodes (AQI in orange, red or purple levels). Forecasts missing warning-triggering episodes (false negatives) are especially problematic in air quality management because the resulting inaction can lead to human exposure to dangerous concentrations of pollutants.

Pollutant	Average time	Average Concentration [$\mu g/m^3$]				
		No warning		Warning		
		Green	Yellow	Orange	Red	Purple
$PM_{2.5}$	24 hours	0-12	13-37	38-55	56-150	$\geq$ 151

Table 3
Air Quality Index (AQI) as defined for the Aburrá Valley with respect to $PM_{2.5}$ concentrations.

[1] available in Spanish https://www.metropol.gov.co/ambiental/calidad-del-aire/Documents/POECA/Plan_de_Acci%C3%B3n_POECA_Metropolitano_2019.pdf. Last accessed, October 2020.

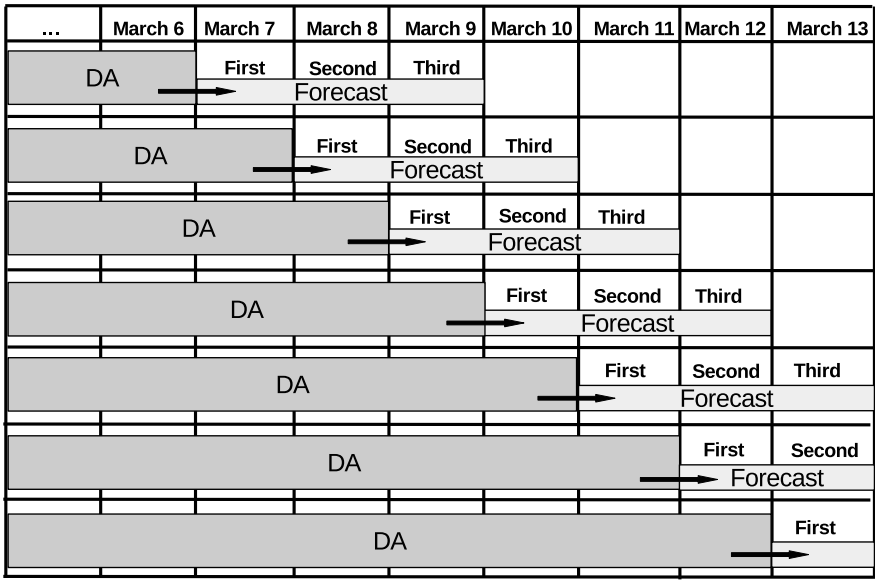

Figure 4: Graphic explanation of the experimental forecast setup. The arrows represent the inheritance of the last correction factor 24-hourly profile into the forecast. All simulations start at February 23 19:00 UTC-5. A spin-up of 5 previous days was taken for each simulation.

3. Results

3.1. Evaluation with low-cost sensor network

The performance of 145 sensors from the low-cost network was evaluated against data from the official network. The remaining 110 sensors did not have an official monitoring station within a 2-km radius. Figure 5 shows the histograms of the MFB, RMSE and R, and the geographical distribution of the performance values. For the majority (67%) of the low-cost sensors an MFB between -0.25 and 0.25 was obtained, with an average of about 0.2. Average RMSE was close to 8 $\mu g/m^3$, with most sensors presenting values below 15 $\mu g/m^3$. The majority (88%) of the sensors showed correlations with R values above 0.7. Observed errors fell within acceptable ranges (as in Boylan and Russell, 2006; Shaocai et al., 2006). Zonal differences in measurement errors were observed. Locations in the South-central part of the city of Medellín (green ellipse on Figure 3.1 (d), (e) y(f)) contained most of the sensors with a R values lower than 0.5 and RMSE values grater than 15 $\mu g/m^3$. Those sensors are located in a dense urban area, while the closest monitoring stations is located in the outskirts of the city. Figure 6 shows the spatial distribution of the complete low-cost network and subset of 115 low-cost sensors with the highest quality data (as defined in section 2.3). The selection of the low-cost high quality is based in the results showed in Figure 3.1(b) and (e).

3.2. Evaluation of data assimilation runs

The concentration fields generated by the model simulations with or without data assimilation were compared to the observations from seven of the official monitoring stations (*validation stations*, green stars in Figure 6) to evaluate the performance of the data assimilation schemes. Figure 7 shows the temporal series for the simulated and observed $PM_{2.5}$ concentrations at four of the validation stations. The four selected stations represent downtown Medellín (station 25), residential areas (station 86), areas with high vehicular flow (station 88), and a peri-urban area in the outskirts of the city (station 85). Those stations summarize the behavior of all seven validation stations. The LE simulation consistently underestimated the concentrations observed at stations 85 and 88. At stations 25 and 86, the LE simulation results were close in magnitude between February 24 and March 3 and March 10 to March 15; between March 3 and March 10, the model presented values much lower than those observed. The day-to-day variability was reduced for this same period, as seen in stations 85 and 86. This inconsistent behavior suggests a poor representation of the meteorological dynamics that govern the dispersion and accumulation of $PM_{2.5}$ within the valley. Simulations using data assimilation showed noisier behaviors than the LE simulation. This process is commonly observed when applying the EnKF and obeys the stochastic nature and the handling of uncertainty inherent to the method (Evensen, 2003). However, those

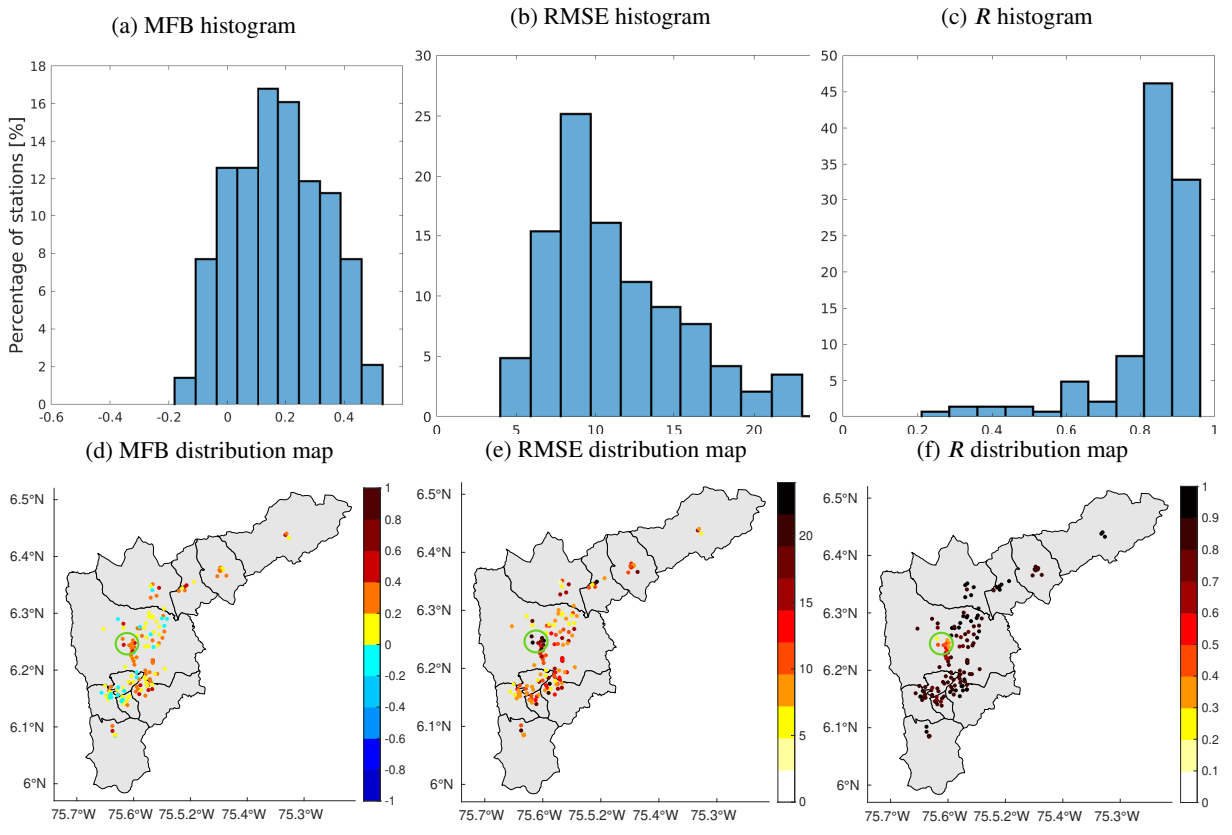

Figure 5: Evaluation of low-costs network against the official monitoring network for the period between 25-February-2019 and 15-March-2019.

simulations managed to correct the large discrepancies present in the LE simulation. Both LE-official, LE-lowcost, and LE-lowcost-HQ represented more accurately the day-to-day variability of the observations than LE. In general terms, there was no evidence of a sizeable and persistent difference among the simulations with data assimilation throughout the entire period. Nevertheless, the LE-lowcost-HQ simulation reproduced with greater accuracy the concentrations observed in different periods, such as between February 26 and March 4 in station 25, between March 9 and March 14 in stations 85 and 86.

Figure 8 shows the diurnal cycles during the simulation period in the four selected validations stations. The diurnal cycle of the LE simulation differed from the observations in both magnitude and temporal behavior. The highest concentration peak that appears around 09:00 in all the stations is mainly due to traffic dynamics. In stations 25 and 88, the LE morning peak corresponded in time but not in magnitude with the observations; in stations 85 and 86, said peak appeared later in the simulations than in the observations. This time lag suggests a poor spatial representation of mobile emissions by the emissions inventory; or a deficiency it the wind fields in reproducing the valley dynamics, showing a late transport of the particulate material to these areas. The LE simulation did not capture the evening peak shown by the observations around 21:00 hours. The simulations using data assimilation presented diurnal cycles closer to the observations than did the LE simulation. The LE-official simulation captured the time and magnitude of the morning peak in stations 85 and 86. In station 88, LE-official corrected the time lag in the morning peak seen in LE, and improved the estimated magnitudes albeit still falling short of the observed values. A different behavior was seen for station 25, where LE-official had low diurnal variability, with a slight underestimation in the morning, and an overestimation in the afternoon. The LE-lowcost and LE-lowcost-HQ simulations results resembled closely the diurnal behavior of the observations, especially the temporal component. In all the stations, both the morning and the evening peaks matched the observations. The observed concentrations for stations 25 and 88 fell inside the standard deviation range for the LE-lowcost simulation; the same simulation overestimated the concentrations between 11:00 and 19:00 for station 85, and underestimated the concentrations between 01:00 and 13:00 for station 86. The LE-lowcost-HQ

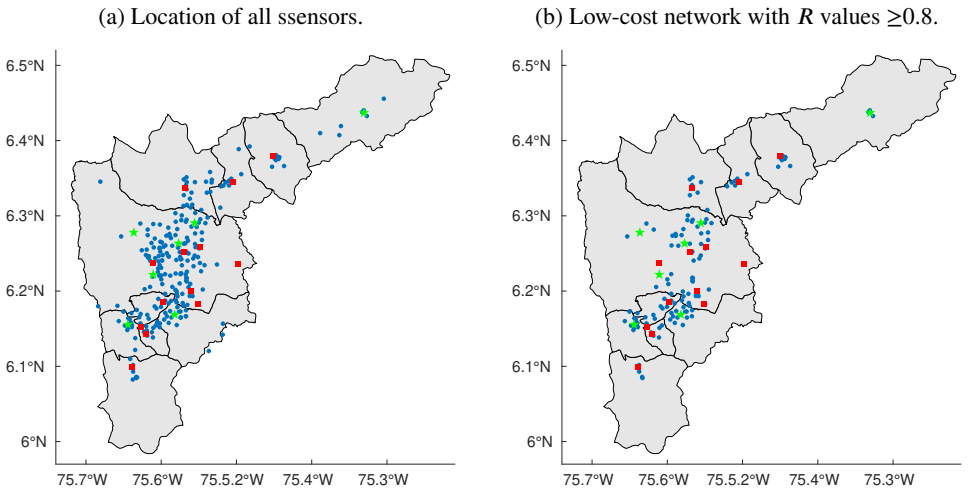

Figure 6: Spatial distribution of the different sets of sensors used for assimilation and validation. Blue dots indicate the location of the low-cost network sensors. Red squares correspond to the locations of the official monitoring stations that were used for data assimilation. Green stars indicate the stations from the official network whose data where used for validation of all model simulations.

simulation results were overall the closest to observations.

The averaged evaluation statistics among all the validation station are shown in Table 4.The simulation results without data assimilation (LE) underestimated the observed concentrations in all the validation stations. This was also seen in previous related works (Lopez-Restrepo et al., 2020; Henao, Mejía, Rendón and Salazar, 2020). The RMSE value reflected a low correspondence between the observed and simulated concentrations when using the model without data assimilation. The correlation coefficient was low, meaning that the model was not able to capture the variations in diurnal and day-to-day concentrations. In contrast, the three simulations using data assimilation had MFB values close to 0, without a significant difference among them. The data assimilation was thus effective in reducing between the model and reality. The RMSE also improved when using data assimilation, decreasing by 24.4% in the LE-official, 32.8% in the LE-lowcost, and 36.2% in the LE-lowcost-HQ simulations relative to the RMSE of the LE simulation. The R values were all above the criteria of good performance according with (Mogollón-sotelo, Belalcazar and Vidal, 2020) Table 2, and based in (EPA, 2000; Boylan and Russell, 2006). Assimilation of either data set from the low-cost network resulted in improved error statistics when compared to the LE-official simulation.

	MFB	RMSE	R
LE	-0.65	27.38	0.42
LE-official	-0.07	20.69	0.64
LE-lowcost	0.08	18.39	0.76
LE-lowcost-HQ	0.06	17.46	0.82

Table 4
Mean Fractional Bias, Root Mean Square Error and Pearson Correlation Coefficient for simulated $PM_{2.5}$. Values are averaged over all the validation stations for the simulation period.

3.3. Evaluation of forecasts

Figure 9 shows a graphical evaluation of the model forecasts for March 12 as day 1, 2 or 3 within the forecasting window. Forecasts for all other days within the forecasting experiment behaved similarly. The observed AQIs and the values for the LE simulation are the same in all the graphs since all graphs illustrate the same calendar day (March 12). Similar to the results shown in section 3.2, the LE simulation underestimated $PM_2.5$ concentrations throughout the valley, yielding in most cases AQI lower than those reported. The AQI forecasts of the three simulations with data assimilation were consistently more accurate than the estimates from the simulation without assimilation (LE). There were no significant differences in performance among the three data assimilation simulations through the three forecast

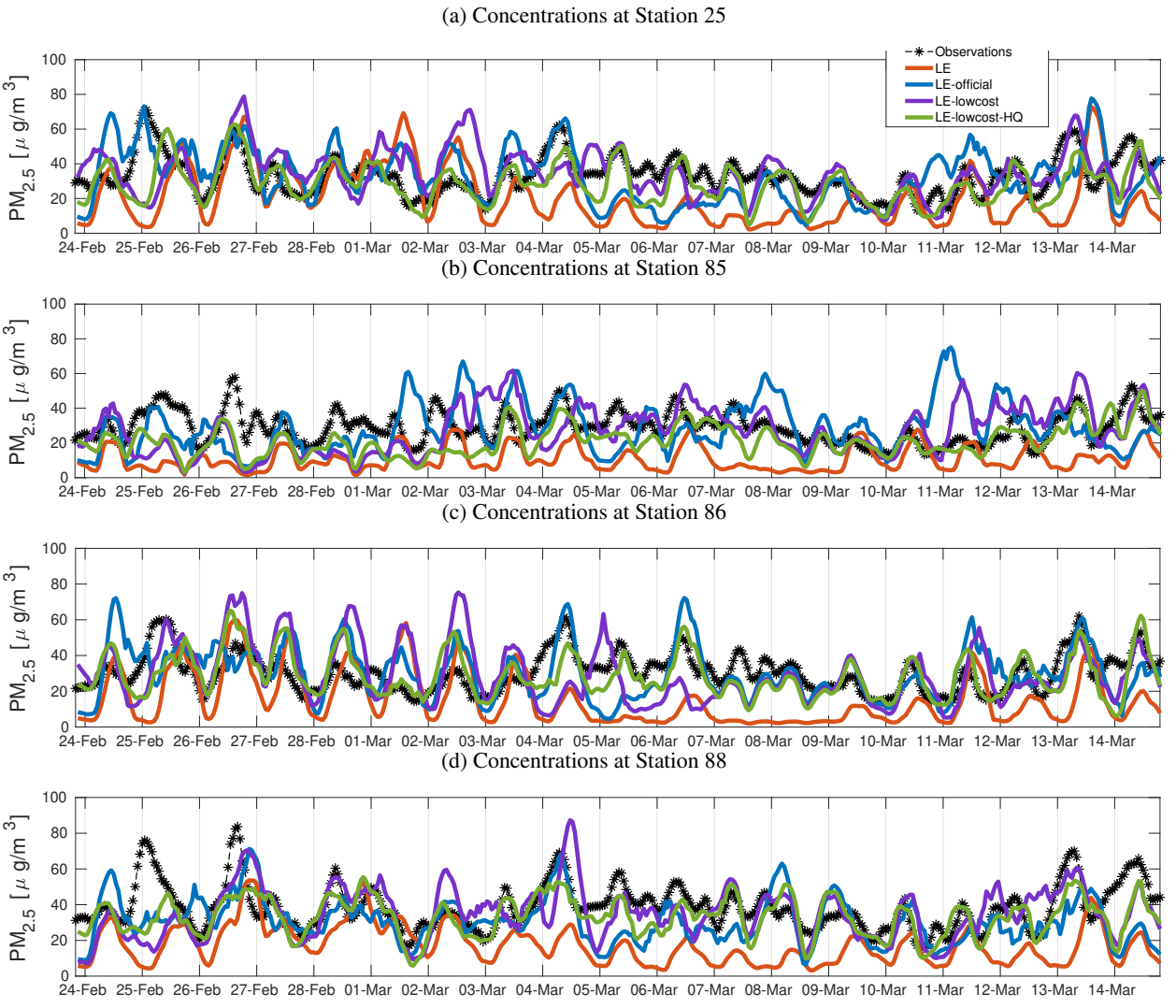

Figure 7: Temporal series of $PM_{2.5}$ concentrations from selected validation stations of the official network, LOTOS-EUROS without assimilation, LE-official, LE-lowcost and LE-lowcost-HQ. Time stamps are valid for local time (UTC-5). A spin-up of 5 previous days was taken for each simulation.

days. Their forecast accuracy decreased as the forecasting window advanced, as could be expected from the uncertainty inherent in the meteorological fields and nominal emission factors. All three simulations with data assimilation had similar spatial behavior, with a tendency to underestimate the AQI in the Northern and Eastern areas of the valley.

For public information on air quality, it is essential that a forecast correctly warns of a critical pollution event. Figure 10 shows the confusion matrix for LE-official, LE-lowcost, and LE-lowcost-HQ simulations in the data assimilation and forecast windows. The confusion matrix summarizes the percentage of true negatives, true positives, false negatives, and false positives (Kohavi and Provost, 1998). The data assimilation evaluation is performed just in the seven validation stations shown in Figure 6. The LE simulation does not offer a warning in any station in the assimilation nor forecast windows; for that reason, its confusion matrix is not presented. In the assimilation window, data assimilation simulations have a percentage of true negatives and true positives higher than 80%, and even higher than 90% in the case of the LE-lowcost-HQ. Both simulations using the low-cost network show lower false negative values than LE-official. The LE-lowcost-HQ has the highest accuracy in reproducing the warning-triggering events within the data assimilation window. The accuracy of the three simulations is lower in the forecast window than in the assimilation window. The small percentage of false positives and high percentage of false negatives suggests that

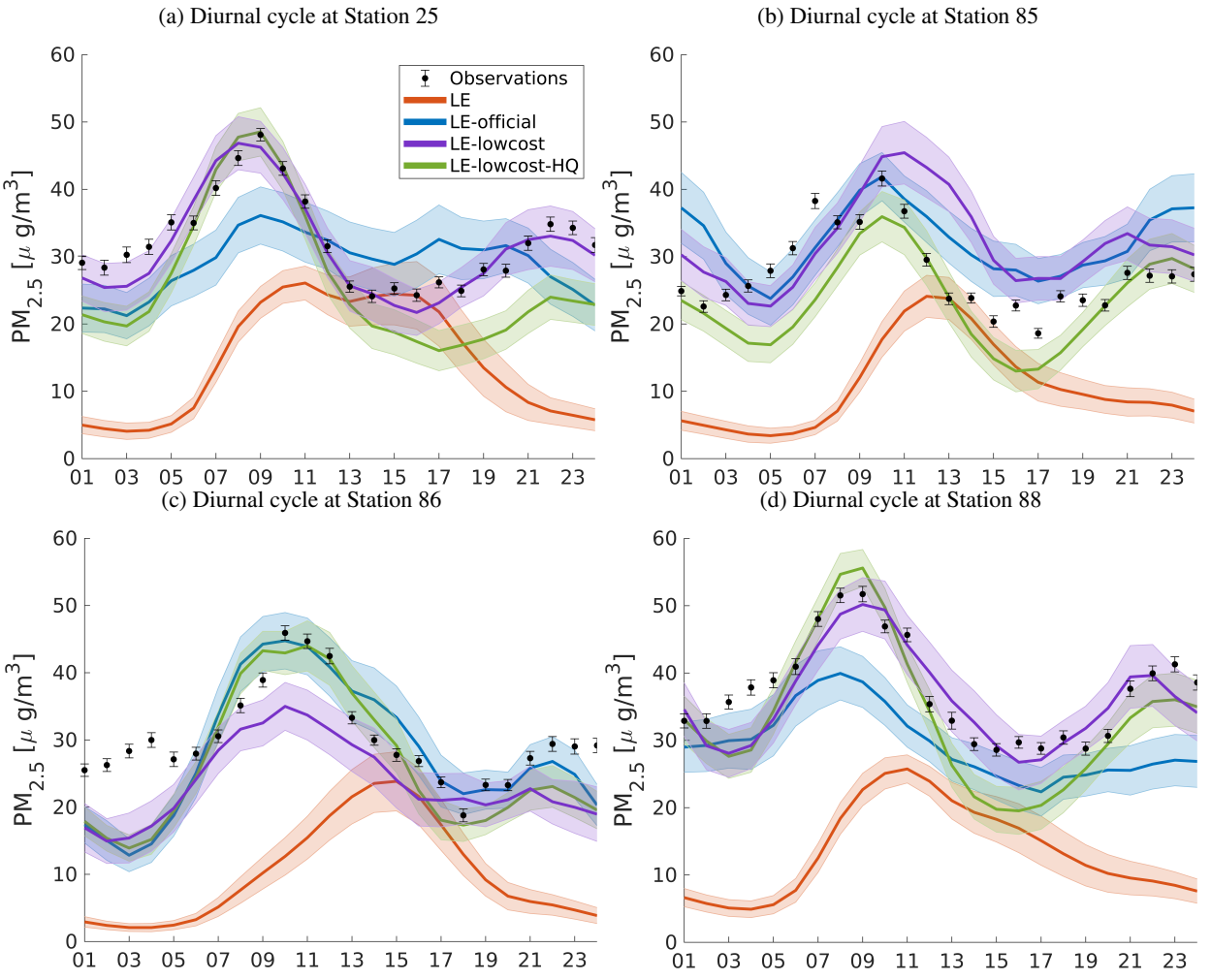

Figure 8: Diurnal cycle of $PM_{2.5}$ concentrations from selection stations of the official network, LOTOS-EUROS without assimilation, LE-official, LE-lowcost and LE-lowcost-HQ. The bars and the shadows represent the standard deviation over the simulation period. The time stamps are valid for local time (UTC-5).

even using the estimated emissions inventory, the simulations continue to underestimate the observations. As observed within the data assimilation window, the two simulations assimilating data from the low-cost network (LE-lowcost and LE-lowcost-HQ) had better warning forecast performance than the LE-official simulation.

4. Discussion and comments

The experiments described in this paper show that it is currently possible to develop low-cost networks with high performance even for cities with air quality problems such as Medellin. The high spatial density of the low-cost network allowed much higher spatial resolution than that attained with the official network. The errors in the low-cost sensors located within the green ellipse in Figure 3.1 (d), (e) and (f) represented spatial outliers. The increased errors observed in this sector of the Valley may be attributed to specific factors such as maintenance, characteristics of the infrastructure in which the sensors are located, differences in elevation relative to the official station against which they were evaluated, or particular meteorological conditions within the subregion of the Valley that may yield local heterogeneity in PM concentrations. Said green ellipse corresponds to a transition zone between peri-urban terrain and an expanding horizon of high-density residential buildings. The low-cost sensors are located in said buildings, while the official monitoring station is located in a school surrounded by forests. This may explain the apparent overestimation of the PM levels by the low-cost sensors and the low correlation values of their data.

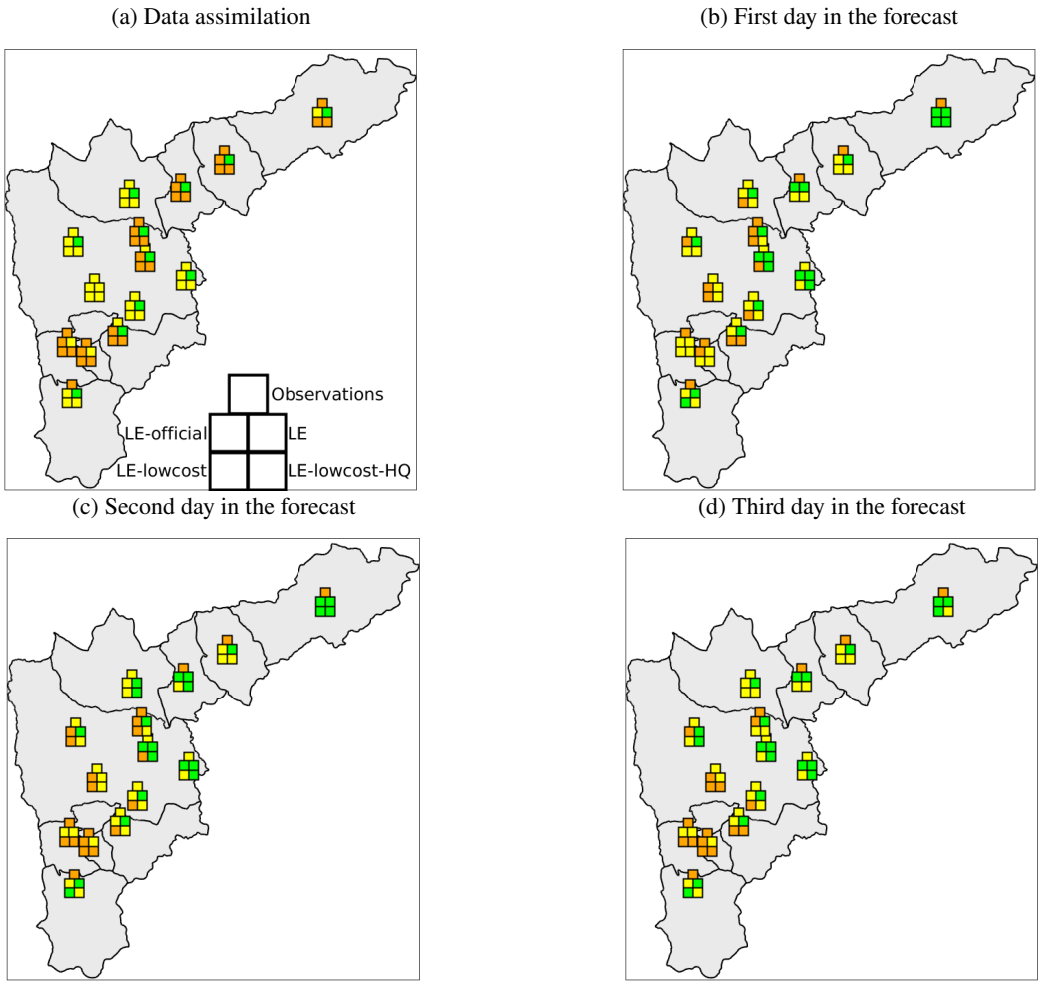

Figure 9: Evaluation of Air Quality Index (AQI) forecast capabilities of LOTOS-EUROS for the Aburrá Valley. All figures represents the forecasts for March 12 when it corresponded to the first (a), second (b) and third (c) day within the forecasting window. The five-square markers are located at the geographical location of each of the official stations used for comparisons. The upper-center square is the AQI calculated from the observed PM values, against which all other values are compared; the middle-left inner square is the AQI predicted by the LE-official simulation; the middle-right inner square is the AQI predicted by the model without assimilation; the bottom-left inner square the AQI predicted by the LE-lowcost simulation; and the bottom-right inner square is the AQI predicted by the LE-lowcost-HQ simulation. The AQI definition is as Table 3.

Our results show a low correlation values and a high underestimation of the observed concentration by the LOTOS-EUROS model without assimilation. Similar behavior were observed in previous works (Lopez-Restrepo et al., 2020; Henao et al., 2020). In (Henao et al., 2020) the WRF-Chem model in a sub-kilometer configuration was used to reproduce the CO dynamics in the valley. The emission inventory was obtained from the AMVA Official Emission Inventory (UPB and AMVA, 2017) and following a methodology similar to the presented in Section 2.2.2. Although the meteorological fields showed a high similarity with observations, the model underestimated the CO concentrations. The underestimation in both cases is attributed to mismatches in the official emission inventory and uncertainties generated by the simplifications of disaggregation methodologies. However, data assimilation notably improves the ability of LOTOS-EUROS to represent the magnitude and dynamics of $P_{2.5}$ within the Aburrá Valley. The assimilation of data from the low-cost network improves the correlation between the observed and the simulated concentrations to a greater extent than when data from the sparse official network is assimilated, both in terms of the RMSE and the R values. The errors left in the simulated concentrations after the assimilation of the low-cost network are within the performance

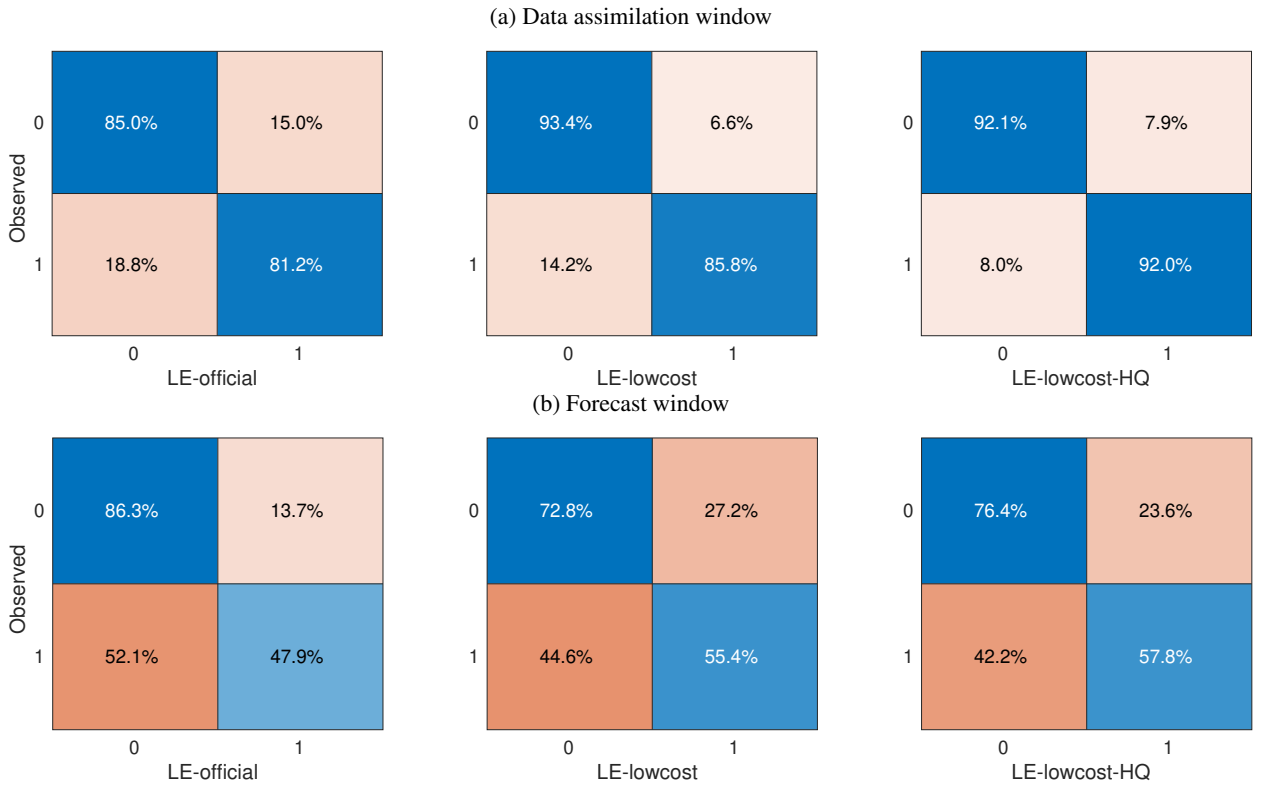

Figure 10: Comparison of confusion matrices for the data assimilation and forecast window depending on warning or no warning per station. The values are calculated across all the days of the corresponding window. The value o 0 corresponds with no warning, the value of 1 corresponds with a warning. For the LE simulation, there are no warnings in the data assimilation window nor forecast windows.

goals for $PM_{2.5}$ representation formulated in (EPA, 2000; Chang and Hanna, 2004; Shaocai et al., 2006; Boylan and Russell, 2006). The uncertainty present in the model causes the percentage of predicted alarm-triggering events related to high concentration of $PM_{2.5}$, to decrease to almost one half of the events observed within the forecasting window (Figure 10). Our results highlight the persistent need to improve the inventories of nominal emissions, the meteorological data used, and to reduce other sources of uncertainty in the model in order to increase forecasting capacity. Nevertheless, the model's forecasting capacity is increased when observations are assimilated. The greater spatial coverage of the low-cost network contributed significantly to the improvements against the simulations assimilating data from the official network. The higher density of observations also allowed estimating emissions in more detail, as seen in Figure 8. The more detailed emission estimations also allowed a better reproduction of the concentrations in the forecast window even in the absence of data assimilation.

Although the LE-lowcost simulation used more observations than the LE-lowcost-HQ simulation (255 and 115, respectively), the location and quality of the additional observations played an important role. The LE-lowcost-HQ was defined using a high similarity criterion to the official network, so it was not as affected by observations with low quality as LE-lowcost. Comparisons between Figure 6 (a) and Figure 6 (b) reveal that the additional locations did not increase the spacial density considerably relative to the low-cost high quality sensors. Our results suggested that while a high observation density is essential for improving the performance of a model with data assimilation, it is crucial to consider other factors such as quality of the data and the location of the sensors. Different techniques of observation localization allow optimizing the number of sensors to improve the data assimilation or other data fusion techniques (Alexanderian, Petra, Stadler and Ghattas, 2016; King, Kang and Xu, 2015; Mazzoleni, Alfonso and Solomatine, 2017; Yildirim, Chryssostomidis and Karniadakis, 2009). We highly recommend implementing these techniques in the development of a new low-cost network. Apart from minimizing the number of sensors and associated costs, the processing of a reduced number of observations requires less computational resources. As an example, the LE-lowcost

simulation was 3.2 times lower than the LE-lowcost-HQ using the same computation configuration. Optimization of computational and time resources are especially important for operational systems.

Jointly with previous work (Johnston, Basford, Bulot, Apetroaie-Cristea, Easton, Davenport, Foster, Loxham, Morris and Cox, 2019; Popoola et al., 2018; Isakov, Arunachalam, Baldauf, Breen, Deshmukh, Hawkins, Kimbrough, Krabbe, Naess, Serre and Valencia, 2019; Ahangar et al., 2019; Schneider et al., 2017; Moltchanov, Levy, Etzion, Lerner, Broday and Fishbain, 2015), our results can support and motivate the development of future low-cost networks and their integration in data fusion applications. According to the literature, North America, Europe, and China concentrate most of the current low-cost implementations, with experimental, citizen, and data dissemination purposes (Kumar and Gurjar, 2019; Morawska, Thai, Liu, Asumadu-Sakyi, Ayoko, Bartonova, Bedini, Chai, Christensen, Dunbabin, Gao, Hagler, Jayaratne, Kumar, Lau, Louie, Mazaheri, Ning, Motta, Mullins, Rahman, Ristovski, Shafiei, Tjondronegoro, Westerdahl and Williams, 2018). In developing countries, a low-cost network, together with a CTM and data assimilation can provide a valuable first approach to monitoring PM without the high cost of an official air quality network.

5. Conclusions

We present a data assimilation application of a hyper-dense low-cost PM network and the chemical transport model LOTOS-EUROS in a urban setting. The low-cost network provided high quality data comparable to those provided by the official monitoring network. The performance of the model with assimilation of the spatially-dense data from the low-cost network improved both in terms of its representation of the observed dynamics, as well as in its forecast capabilities, highlighting its value as an air-quality management tool. Our results support the idea than with the current advances in the low-cost sensors, it is possible to use low-cost networks and data assimilation to model and predict air quality in urban areas.

Although one of the main advantages of a low-cost networks is the possibility of implemented hyper-dense networks with relative low costs, it is recommended to prioritize in the quality of the data (sensor quality, calibration, maintenance) and the study of optimal localization. High quality and the correct number and localization of sensors improve the data assimilation process and minimizes operational and computational costs.

CRediT authorship contribution statement

Santiago Lopez-Restrepo: Conceptualization, Methodology, Software, Writing - Original Draft. **Andres Yarce:** Methodology, Software. **Nicolás Pinel:** Conceptualization, Methodology, Writing - Review & Editing. **O. L. Quintero:** Conceptualization, Methodology, Writing - Original Draft. **Arjo Segers:** Methodology, Software, Writing - Review & Editing. **A. W. Heemink:** Writing - Review & Editing, Supervision.

Acknowledgement

The authors acknowledge the supercomputing resources made available by the Centro de Computación Científica Apolo at Universidad EAFIT (http://www.eafit.edu.co/apolo) to conduct this work.

References

Ahangar, F.E., Freedman, F.R., Venkatram, A., 2019. Using low-cost air quality sensor networks to improve the spatial and temporal resolution of concentration maps. International Journal of Environmental Research and Public Health 16. doi:10.3390/ijerph16071252.

Alexanderian, A., Petra, N., Stadler, G., Ghattas, O., 2016. A fast and scalable method for a-optimal design of experiments for infinite-dimensional bayesian nonlinear inverse problems. SIAM Journal on Scientific Computing 38, A243–A272. URL: https://doi.org/10.1137/140992564, doi:10.1137/140992564, arXiv:https://doi.org/10.1137/140992564.

Boylan, J.W., Russell, A.G., 2006. Pm and light extinction model performance metrics, goals, and criteria for three-dimensional air quality models. Atmospheric Environment 40, 4946 – 4959. doi:https://doi.org/10.1016/j.atmosenv.2005.09.087. special issue on Model Evaluation: Evaluation of Urban and Regional Eulerian Air Quality Models.

Chai, T., Draxler, R.R., 2014. Root mean square error (rmse) or mean absolute error (mae): Arguments against avoiding rmse in the literature. Geoscientific Model Development 7, 1247–1250. doi:10.5194/gmd-7-1247-2014.

Chang, J.C., Hanna, S.R., 2004. Air quality model performance evaluation. Meteorology and Atmospheric Physics 87, 167–196. doi:10.1007/s00703-003-0070-7.

EPA, 2000. Meteorological Monitoring Guidance for Regulatory Modeling Applications. Technical Report. U.S. ENVIRONMENTAL PROTECTION AGENCY.

Evensen, G., 2003. The Ensemble Kalman Filter: Theoretical formulation and practical implementation. Ocean Dynamics 53, 343–367. doi:10.1007/s10236-003-0036-9.

Gómez, C.D., González, C.M., Osses, M., Aristizábal, B.H., 2018. Spatial and temporal disaggregation of the on-road vehicle emission inventory in a medium-sized Andean city. Comparison of GIS-based top-down methodologies. Atmospheric Environment 179, 142–155. URL: https://doi.org/10.1016/j.atmosenv.2018.01.049, doi:10.1016/j.atmosenv.2018.01.049.

Haklay, M., Weber, P., 2008. Openstreetmap: User-generated street maps. IEEE Pervasive Computing 7, 12–18.

Henao, J.J., Mejía, J.F., Rendón, A.M., Salazar, J.F., 2020. Sub-kilometer dispersion simulation of a CO tracer for an inter-Andean urban valley. Atmospheric Pollution Research , 0–1URL: https://doi.org/10.1016/j.apr.2020.02.005, doi:10.1016/j.apr.2020.02.005.

Hoyos, C.D., Herrera-Mejía, L., Roldán-Henao, N., Isaza, A., 2019. Effects of fireworks on particulate matter concentration in a narrow valley: the case of the medellín metropolitan area. Environmental Monitoring and Assessment 192, 6. URL: https://doi.org/10.1007/s10661-019-7838-9, doi:10.1007/s10661-019-7838-9.

Isakov, V., Arunachalam, S., Baldauf, R., Breen, M., Deshmukh, P., Hawkins, A., Kimbrough, S., Krabbe, S., Naess, B., Serre, M., Valencia, A., 2019. Combining dispersion modeling and monitoring data for community-scale air quality characterization. Atmosphere 10. doi:10.3390/atmos10100610.

Jazwinski, A., 1970. Stochastic processes and filtering theory. Number 64 in Mathematics in science and engineering, Acad. Press, New York, NY [u.a.].

Johnston, S.J., Basford, P.J., Bulot, F.M., Apetroaie-Cristea, M., Easton, N.H., Davenport, C., Foster, G.L., Loxham, M., Morris, A.K., Cox, S.J., 2019. City scale particulate matter monitoring using LoRaWAN based air quality IoT devices. Sensors (Switzerland) 19, 1–20. doi:10.3390/s19010209.

King, S., Kang, W., Xu, L., 2015. Observability for optimal sensor locations in data assimilation. International Journal of Dynamics and Control 3, 416–424. URL: https://www.scopus.com/inward/record.uri?eid=2-s2.0-84975217716&doi=10.1007%2fs40435-014-0120-7&partnerID=40&md5=0ed9184ad57b7b9f7a5413beacfba5f5, doi:10.1007/s40435-014-0120-7. cited By 5.

Kohavi, R., Provost, F., 1998. Applications of Machine Learning and the Knowledge. Applications of Machine Learning and the Knowledge in Machine Learning 30, 349–354.

Kumar, A., Gurjar, B.R., 2019. Low-Cost Sensors for Air Quality Monitoring in Developing Countries - A Critical View. Asian Journal of Water, Environment and Pollution 16, 65–70. doi:10.3233/AJW190021.

Lahoz, W.a., Schneider, P., 2014. Data assimilation: making sense of Earth Observation. Frontiers in Environmental Science 2, 1–28. doi:10.3389/fenvs.2014.00016.

Liu, H.Y., Bartonova, A., Schindler, M., Sharma, M., Behera, S.N., Katiyar, K., Dikshit, O., 2013. Respiratory disease in relation to outdoor air pollution in kanpur, india. Archives of Environmental & Occupational Health 68, 204–217. doi:10.1080/19338244.2012.701246.

Liu, H.Y., Dunea, D., Iordache, S., Pohoata, A., 2018. A review of airborne particulate matter effects on young children's respiratory symptoms and diseases. Atmosphere 9. URL: https://www.mdpi.com/2073-4433/9/4/150, doi:10.3390/atmos9040150.

Liu, H.Y., Schneider, P., Haugen, R., Vogt, M., 2019. Performance assessment of a low-cost PM 2.5 sensor for a near four-month period in Oslo, Norway. Atmosphere 10. doi:10.3390/atmos10020041.

Lopez-Restrepo, S., Yarce, A., Pinel, N., Quintero, O., Segers, A., Heemink, A., 2020. Forecasting PM_{10} and $PM_{2.5}$ in the Aburrá Valley (Medellín, Colombia) via EnKF based Data Assimilation. Atmospheric Environment 232, 117507.

Manders, A.M.M., Builtjes, P.J.H., Curier, L., Denier Van Der Gon, H.A.C., Hendriks, C., Jonkers, S., Kranenburg, R., Kuenen, J.J.P., Segers, A.J., Timmermans, R.M.A., Visschedijk, A.J.H., Kruit, R.J.W., Addo, W., Van Pul, J., Sauter, F.J., Van Der Swaluw, E., Swart, D.P.J., Douros, J., Eskes, H., Van Meijgaard, E., Van Ulft, B., Van Velthoven, P., Banzhaf, S., Mues, A.C., Stern, R., Fu, G., Lu, S., Heemink, A., Van Velzen, N., Schaap, M., 2017. Curriculum vitae of the LOTOS–EUROS (v2.0) chemistry transport model. Geosci. Model Dev 10, 4145–4173. doi:10.5194/gmd-10-4145-2017.

Mazzoleni, M., Alfonso, L., Solomatine, D., 2017. Influence of spatial distribution of sensors and observation accuracy on the assimilation of distributed streamflow data in hydrological modelling. Hydrological Sciences Journal 62, 389–407. URL: https://www.scopus.com/inward/record.uri?eid=2-s2.0-84992702872&doi=10.1080%2f02626667.2016.1247211&partnerID=40&md5=51640746a8e2b764b797fe44811ef7cf, doi:10.1080/02626667.2016.1247211. cited By 6.

Mogollón-sotelo, C., Belalcazar, L., Vidal, S., 2020. A support vector machine model to forecast ground-level $pm_{2.5}$ in a highly populated city with a complex terrain. Air Quality, Atmosphere & Health .

Moltchanov, S., Levy, I., Etzion, Y., Lerner, U., Broday, D.M., Fishbain, B., 2015. On the feasibility of measuring urban air pollution by wireless distributed sensor networks. Science of the Total Environment 502, 537–547. URL: http://dx.doi.org/10.1016/j.scitotenv.2014.09.059, doi:10.1016/j.scitotenv.2014.09.059.

Morawska, L., Thai, P.K., Liu, X., Asumadu-Sakyi, A., Ayoko, G., Bartonova, A., Bedini, A., Chai, F., Christensen, B., Dunbabin, M., Gao, J., Hagler, G.S., Jayaratne, R., Kumar, P., Lau, A.K., Louie, P.K., Mazaheri, M., Ning, Z., Motta, N., Mullins, B., Rahman, M.M., Ristovski, Z., Shafiei, M., Tjondronegoro, D., Westerdahl, D., Williams, R., 2018. Applications of low-cost sensing technologies for air quality monitoring and exposure assessment: How far have they gone? Environment International 116, 286–299. doi:10.1016/j.envint.2018.04.018.

Mues, a., Kuenen, J., Hendriks, C., Manders, a., Segers, a., Scholz, Y., Hueglin, C., Builtjes, P., Schaap, M., 2014. Sensitivity of air pollution simulations with LOTOS-EUROS to the temporal distribution of anthropogenic emissions. Atmospheric Chemistry and Physics 14, 939–955. doi:10.5194/acp-14-939-2014.

Ossés de Eicker, M., Zah, R., Triviño, R., Hurni, H., 2008. Spatial accuracy of a simplified disaggregation method for traffic emissions applied in seven mid-sized Chilean cities. Atmospheric Environment 42, 1491–1502. doi:10.1016/j.atmosenv.2007.10.079.

Ott, E., Hunt, B.R., Szunyogh, I., Zimin, A.V., Kostelich, E., Corazza, M., Kalnay, E., Patil, D., Yorke, J.A., 2004. A local ensemble Kalman filter for atmospheric data assimilation. Tellus 56, 415–428.

Popoola, O.A., Carruthers, D., Lad, C., Bright, V.B., Mead, M.I., Stettler, M.E., Saffell, J.R., Jones, R.L., 2018. Use of networks of low cost air quality sensors to quantify air quality in urban settings. Atmospheric Environment 194, 58–70. doi:10.1016/j.atmosenv.2018.09.030.

Pournazeri, S., Tan, S., Schulte, N., Jing, Q., Venkatram, A., 2014. A computationally efficient model for estimating background concentrations of nox, no2, and o3. Environmental Modelling and Software 52, 19 – 37. URL: http://www.sciencedirect.com/science/article/pii/S1364815213002612, doi:https://doi.org/10.1016/j.envsoft.2013.10.018.

Sakov, P., Evensen, G., Bertino, L., 2010. Asynchronous data assimilation with the EnKF. Tellus, Series A: Dynamic Meteorology and Oceanography 62, 24–29. doi:10.1111/j.1600-0870.2009.00417.x.

Sauter, F., der Swaluw, E.V., Manders-groot, A., Kruit, R.W., Segers, A., Eskes, H., 2012. TNO report TNO-060-UT-2012-01451. Technical Report. TNO. Utrecht, Netherlands.

Schneider, P., Castell, N., Vogt, M., Dauge, F.R., Lahoz, W.A., Bartonova, A., 2017. Mapping urban air quality in near real-time using observations from low-cost sensors and model information. Environment International 106, 234–247. URL: http://dx.doi.org/10.1016/j.envint.2017.05.005, doi:10.1016/j.envint.2017.05.005.

Shaocai, Y., Brian, E., Robin, D., Shao-Hang, C., E., S.S., 2006. New unbiased symmetric metrics for evaluation of air quality models. Atmospheric Science Letters 7, 26–34. doi:10.1002/asl.125.

Tippett, M.K., Anderson, J.L., Bishop, C.H., Hamill, T.M., Whitaker, J.S., 2003. Ensemble square root filters. Monthly Weather Review 131, 1485–1490. doi:10.1175/1520-0493(2003)131<1485:ESRF>2.0.CO;2.

Tuia, D., Ossés de Eicker, M., Zah, R., Osses, M., Zarate, E., Clappier, A., 2007. Evaluation of a simplified top-down model for the spatial assessment of hot traffic emissions in mid-sized cities. Atmospheric Environment 41, 3658–3671. doi:10.1016/j.atmosenv.2006.12.045.

UPB, AMVA, 2017. Inventario de Emisiones Atmosféricas del Valle de Aburrá - actualización 2015. Technical Report. Universidad Pontificia Bolivariana - Grupo de Investigaciones Ambientales, Area Metropolitana del Valle de Aburra. Medellín. URL: https://www.metropol.gov.co/ambiental/calidad-del-aire/Documents/Inventario-de-emisiones.

Van Loon, M., Builtjes, P.J.H., Segers, a.J., 2000. Data assimilation of ozone in the atmospheric transport chemistry model LOTOS. Environmental Modelling and Software 15, 603–609. doi:10.1016/S1364-8152(00)00048-7.

Yildirim, B., Chryssostomidis, C., Karniadakis, G., 2009. Efficient sensor placement for ocean measurements using low-dimensional concepts. Ocean Modelling 27, 160–173. URL: https://www.scopus.com/inward/record.uri?eid=2-s2.0-61449136716&doi=10.1016%2fj.ocemod.2009.01.001&partnerID=40&md5=8f4eab5a692db6cf440aeb04f8269b71, doi:10.1016/j.ocemod.2009.01.001. cited By 55.